Ann Nucl Med (2010) 24:507–514
DOI 10.1007/s12149-010-0388-4

ORIGINAL ARTICLE

Importance of gated CT acquisition for the quantitative improvement of the gated PET/CT in moving phantom

Y. Sakaguchi · T. Mitsumoto · T. Zhang · K. Mitsumoto · Y. Tachiya · N. Ohya · M. Sasaki

Received: 4 March 2010 / Accepted: 25 April 2010 / Published online: 12 June 2010

Abstract
Objective The aim of this study was to investigate the utility of gated PET/CT and CT attenuation correction (AC) for the quantitation of radioactivity.
Methods An ellipse phantom containing six spheres, ranging from 10 to 37 mm in diameter, was filled with 36.7 kBq/mL of F-18. The respiratory motion was simulated by a motor-driven plastic platform to move the phantom with a displacement of 2 cm in the craniocaudal direction at a frequency of 15/min. With the phantom at rest, PET/CT data were acquired and used as a standard (nonmotion). With the phantom in motion, PET data were acquired in both the static and gated modes (sPET and gPET, respectively). Helical CT (HCT), slow CT (SCT), average CT (ACT), and four-dimensional CT (4DCT) were acquired and used to correct attenuation. On both PET and CT images, the maximum radioactivity, dimensions, and CT numbers were measured on the central slices.
Results In nonmotion, recovery coefficients whose spheres were 22 mm or smaller gradually decreased. Regarding motion, the PET counts of the spheres in the static acquisition were lower than those acquired in nonmotion with either type of CTAC (sPET–HCT: −43.8%, sPET–SCT: −51.4%, sPET–ACT: −49.5%). Gated acquisition of PET significantly improved the PET counts (gPET–HCT: −30.1%) ($p < 0.05$), while additional gated acquisition of CT significantly improved them further (gPET–4DCT: −15.2%) ($p < 0.01$). The dimensions of sPET were overestimated, but those of gPET were close to the standard values. The SCT significantly overestimated the dimensions, and the water density area decreased ($p < 0.01$). The 4DCT images were similar to the HCT images.
Conclusions In respiratory motion, PET acquisition in the static mode underestimated the radioactivity and overestimated the dimensions. Neither SCT nor ACT improved these errors. Although PET acquisition in the gated mode improved the quantification of PET/CT images, the additional gated CT acquisition using 4DCT is required for further improvement.

Keywords Respiration motion · Gated · PET/CT · 4DCT · Attenuation correction

Y. Sakaguchi · T. Mitsumoto · T. Zhang · M. Sasaki (✉)
Division of Radiological Science, Department of Health Sciences, Graduate School of Medical Sciences, Kyushu University, 3-1-1 Maidashi, Higashi-ku, Fukuoka 812-8582, Japan
e-mail: msasaki@shs.kyushu-u.ac.jp

K. Mitsumoto · Y. Tachiya
Radiological Science Course, Department of Health Sciences, School of Medicine, Kyushu University, Fukuoka, Japan

N. Ohya
Department of Medical Technology, Kyushu University Hospital, Fukuoka, Japan

Introduction

PET/CT, which provides anatomical and functional information, can be useful for tumor diagnosis, particularly regarding differential diagnosis, staging, response evaluation, and prognosis [1]. However, PET emission data acquisition is required for a few minutes per bed and also consists of several respiratory cycles. Therefore, the usual PET images are taken over an averaged state of respiration. The respiration-averaged PET images result in an underestimation of radioactivity and an overestimation of tumor volume in the thoracic and abdominal regions, especially in

the vicinity of the diaphragm [2]. The underestimation of radioactivity increases the incidence of false-negative results. Some faint accumulations are not visible on images, and the standardized uptake values (SUV) of some lesions become low. Furthermore, the difference in temporal resolution results in a spatial misalignment between PET and CT data [3, 4].

To eliminate spatial misalignment between PET and CT images in motion objects, the averaging of CT images over respiratory phases has been proposed. Slow CT (SCT) is acquired with a long gantry rotation time that includes several respiratory cycles [5, 6]. Average CT (ACT) images were developed by averaging the CT images in all respiratory phases observed by four-dimensional CT (4DCT) acquisition in the cine mode [7]. These blurred CT images are reported to minimize misregistration between the CT attenuation correction (CTAC) and PET data acquired in static mode [6, 7]. Another method is gated acquisition to eliminate the effect of respiratory motion for PET emission data [8]. In the gated-acquisition protocol, PET emission data are continuously acquired in list mode as respiratory motion is monitored. The data are divided into several respiratory phases and are used to reconstruct PET/CT images of each respiratory phase. In addition, 4DCT was developed to better register CT and PET data acquired in gated mode [9]. 4DCT is acquired in cine mode using the respiratory system and is divided into phases similar to those of gated PET [10]. However, the effect of the combination of PET acquisition mode and CTAC has not yet been evaluated.

The purpose of this study is to assess the usefulness of gated CT acquisition for the quantification of PET/CT by comparing the different acquisition protocols using a moving hot sphere phantom.

Materials and methods

Phantom and motion tables

The National Electrical Manufacturers Association (NEMA) 2001 International Electrotechnical Commission (IEC) phantom (Data Spectrum Corp., Hillsborough, NC) consisting of a quasicylindrical cavity (280 × 210 × 180 mm) and six spheres (Model ECT/IEC -BODY/P) was used for this study. The spheres were 10, 13, 17, 22, 28, and 37 mm in diameter, and their wall thickness was 1 mm. All of the spheres were filled with ^{18}F solution of 36.7 kBq/mL, and the background was filled with air. The radioactivity was equal to SUV = 15. A newly designed motion system was used in this study to simulate respiratory motion. The NEMA phantom was placed on a moving table, and a motor-driven table oscillated with a displacement of 2 cm in the craniocaudal direction and a frequency of 15/min. The parameters were selected to simulate displacements and respiratory cycles typically observed in normal respiratory motion.

The motion tracking was recorded by a real-time position management (RPM) respiratory gating system (Varian Medical Systems, Palo Alto, CA). The motion was sinusoidal. A trigger was set at a defined phase within the respiratory cycle and initiated the acquisition cycle in gated PET and dynamic CT. Finally, the respiratory cycles were divided into eight phases.

Data acquisition

PET/CT scans were acquired in both a nonmoving status (nonmotion) and a moving status (motion) on a Discovery ST Elite (GE Healthcare, Milwaukee, WI). The 16-slice CT scanning parameters were 120 kV, 30–154 mA, matrix 512 × 512, slice thickness 5 mm, and transaxial field of view 500 mm. Gantry rotation was 0.5 s/rotation for conventional helical CT (HCT), 5.0 s/rotation for SCT, and 0.5 s/rotation in the cine mode for ACT and 4DCT. The HCT was performed in a nonmoving status with spheres placed at the center position of movement, which is the midpoint between phases 2 and 3. A 5 s cine duration time and a 0.45 s interval time between image reconstructions were used as the cine mode parameters. The total scan length was set to cover the full displacement of the phantom. The ACT data sets were generated based on fixed cine duration image averaging. However, the ACT images were not available.

Emission data were acquired in the 3D mode with 128 × 128 matrices (5.47 × 5.47 × 3.27 mm). The acquisition times per bed position were 3 min in static mode and 8 min in gated mode. PET was reconstructed using a 3D ordered subsets-expectation maximization (3D-OSEM) algorithm [VUE Point Plus, 2 iterations, 28 subsets, and a post-filter of 6 mm full width at half maximum (FWHM)].

The PET/CT images in nonmotion scans were reconstructed with a combination of static PET and helical CT data and were used as a standard. The static PET (sPET) in motion was reconstructed with HCT, SCT, and ACT, and the gated PET (gPET) was reconstructed with HCT and 4DCT.

Data analysis

For the PET data, the maximum radioactivity and the dimensions of each sphere were measured on each central coronal slice using a region of interest (ROI). On the monitor displaying PET images, upper and lower SUV were set to 6.0 and 0.0, respectively, according to routine clinical use. To measure the maximum counts of the

sphere, the circular ROI equal to the known sphere size was placed to delineate the sphere under careful visual observation. The ROI must include the area of highest activity. The dimensions of each sphere were measured by manual delineation of the sphere images during the visual assessment. To evaluate the quantification of the PET data, recovery coefficient (RC), %counts, and %dimensions were calculated by:

$$\mathrm{RC} = C_\mathrm{i}/C_\mathrm{r} \times 100$$

$$\%\ \mathrm{counts} = (C_\mathrm{i} - C_\mathrm{r})/C_\mathrm{r} \times 100$$

$$\%\ \mathrm{dimensions} = (D_\mathrm{i} - D_\mathrm{r})/D_\mathrm{r} \times 100$$

where C_i and D_i are interest values, and C_r and D_r are reference values. As a reference for each parameter, the maximum radioactivity of the 37 mm sphere in nonmotion, that of each sphere in nonmotion, and the actual inside dimensions of each sphere were used.

For the CT images, the dimensions and the CT number of spheres were measured on a center slice of each coronal image using a manually placed ROI that delineated the outside surface of each sphere. The %dimensions and %numbers of the CT images were calculated to evaluate the CT data as CTAC. The %dimensions were defined in the same way as PET data. The CT number of pixels in each sphere was segmentally classified into two categories: water density (from −30 HU to 30 HU) and noise density (from −800 HU to −30 HU), using the profile curves of the CT images. The %numbers were the ratio of the number of pixels with each CT number to that of all pixels in the ROI. As a reference for %dimensions and %numbers, the actual outside dimensions and the number of all pixels in the ROI of each sphere were used.

Statistical analysis

Multiple comparisons of the %counts, %dimensions, and %numbers among the difference acquisition protocols were performed using the Tukey–Kramer method. The levels of significance were set at $p < 0.05$ and $p < 0.01$.

Results

Comparison of PET counts

The RC curve of each examination is shown in Fig. 1. The top curve represents the RC of the nonmotion static PET. The gradual decrease of the RC was observed in spheres with diameters of 22 mm or smaller. For the RCs in motion, the sPET–HCT decreased markedly, and the 10 mm sphere was not observed. The RCs of sPET–SCT were lower than those of sPET–HCT. The RCs of sPET–ACT were similar to those of sPET–SCT. On the other hand, the gPET–HCT showed improvement of RCs, and the gPET–4DCT improved further.

The PET count of each sphere in the different acquisition protocols was compared with that of sPET–HCT in the nonmotion status and was expressed as %counts (Table 1). The %counts of the sPET–HCT, sPET–SCT, and sPET–

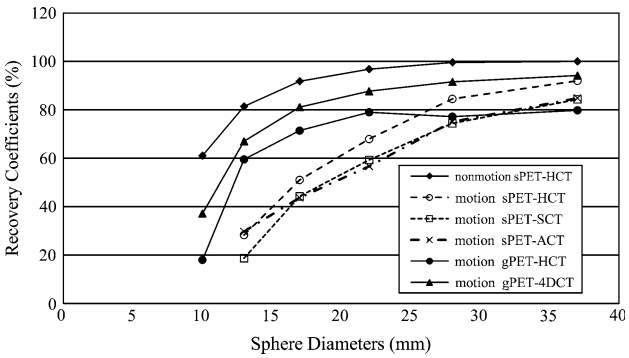

Fig. 1 The RC curves of differences in PET/CT acquisitions. The maximum radioactivity of the 37 mm sphere in nonmotion sPET/HCT is used as a reference. The smaller the sphere size, the lower the RC. In motion sPET, a sphere with a diameter of 10 mm cannot be visualized

Table 1 Comparison of PET counts in different PET/CT protocols

	Sphere diameters (mm)						Mean
	10	13	17	22	28	37	
sPET–HCT	–	−65.3	−44.4	−29.8	−15.1	−8.0	−43.8*
sPET–SCT	–	−77.1	−51.7	−38.7	−25.2	−15.7	−51.4**
sPET–ACT	–	−63.50	−52.37	−41.46	−24.58	−15.21	−49.5***
gPET–HCT	−70.5	−26.9	−22.1	−18.4	−22.5	−20.2	−30.1
gPET–4DCT	−39.0	−17.7	−11.6	−9.5	−8.0	−5.8	−15.2

The numbers are the %counts in comparison to the PET counts of sPET–HCT in the nonmotion status

* The mean %counts of the sPET–HCT were significantly lower than those of gPET–4DCT ($p < 0.01$)

** The mean %counts of the sPET–SCT were significantly lower than those of gPET–HCT ($p < 0.05$) and gPET–4DCT ($p < 0.01$)

*** The mean %counts of the sPET–ACT were significantly lower than those of gPET–HCT ($p < 0.05$) and gPET–4DCT ($p < 0.01$)

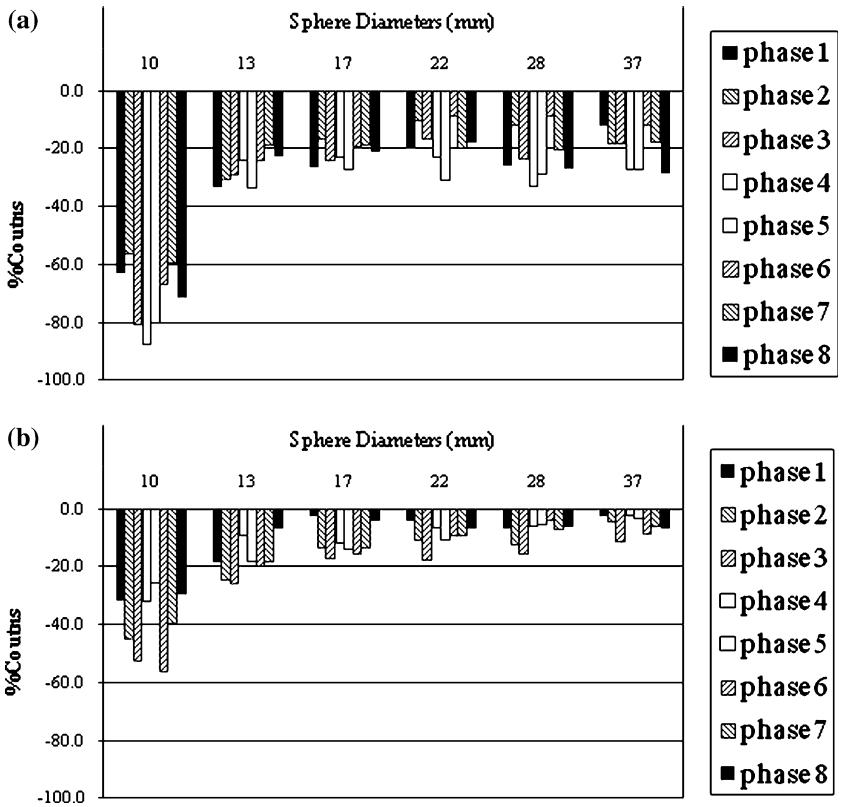

Fig. 2 The %counts of the gated PET in each respiratory phase. **a** gPET–HCT, **b** gPET–4DCT

ACT decreased, especially in the small spheres; their respective mean %counts were −43.8, −51.4, and −49.5%, respectively. On the other hand, the degrees of decrease in the %counts of the gPET–HCT and the gPET–4DCT were mild relative to that of the sPET. The mean %counts of the gPET–HCT and the gPET–4DCT improved to −30.1 and −15.2%, respectively.

The %counts of the gPET–HCT and the gPET–4DCT in each respiratory phase are shown in Fig. 2. In gPET–HCT, the %counts of the central phases (phases 2, 3, 6, and 7) were smaller than those of edge phases (phases 1, 4, 5, and 8). The sphere position during the HCT scan was the midpoint between phases 2 and 3. On the other hand, the %counts of edge phases (phases 1, 4, 5, and 8) were smaller than those of central phases (phases 2, 3, 6, and 7). Figure 3 shows the gated PET and CT images in each respiratory phase. In the gPET–HCT images, the distribution of radioactivity was not homogeneous. The hot area was located in the center position of the respiratory movement where the sphere was placed during HCT scanning. In gPET–4DCT, the distribution of radioactivity was homogeneous.

Comparison of the sphere dimensions

The sphere dimensions of the CT and PET images are shown in Table 2 and Fig. 4. The %dimensions of sPET–HCT (89.7%), sPET–SCT (82.4%), and sPET–ACT (84.5%) were significantly higher than those of nonmotion ($p < 0.01$), gPET–HCT ($p < 0.05$), and gPET–4DCT ($p < 0.05$). However, those of gPET–HCT (28.1%) and gPET–4DCT (24.9%) were close to the standard values. Considering the sphere dimensions on the CT images, the dimensions of the SCT were significantly higher than the standard values ($p < 0.01$). Those of the 4DCT were also close to the standard values.

Comparison of sphere density

The %numbers of the water density and that of the noise density are shown in Fig. 5. The %numbers of the water density of SCT in motion were significantly lower than that of the nonmotion HCT ($p < 0.01$). Those of 4DCT also decreased significantly ($p < 0.01$), while the degree of decrease was milder than in those of SCT. The %numbers of the noise density of SCT in motion significantly increased ($p < 0.01$). Although that of 4DCT also increased significantly, it was lower than that of SCT ($p < 0.01$). The smaller the sphere size, the greater the increase in the %numbers of the noise density. Representative images are shown in Fig. 4.

The %numbers of 4DCT in each respiratory phase are shown in Fig. 6. In 4DCT, the mean %numbers of the water density decreased and that of the noise density increased in the central phases. However, those of both the water and noise densities in the edge phases were close to those of the HCT in nonmotion.

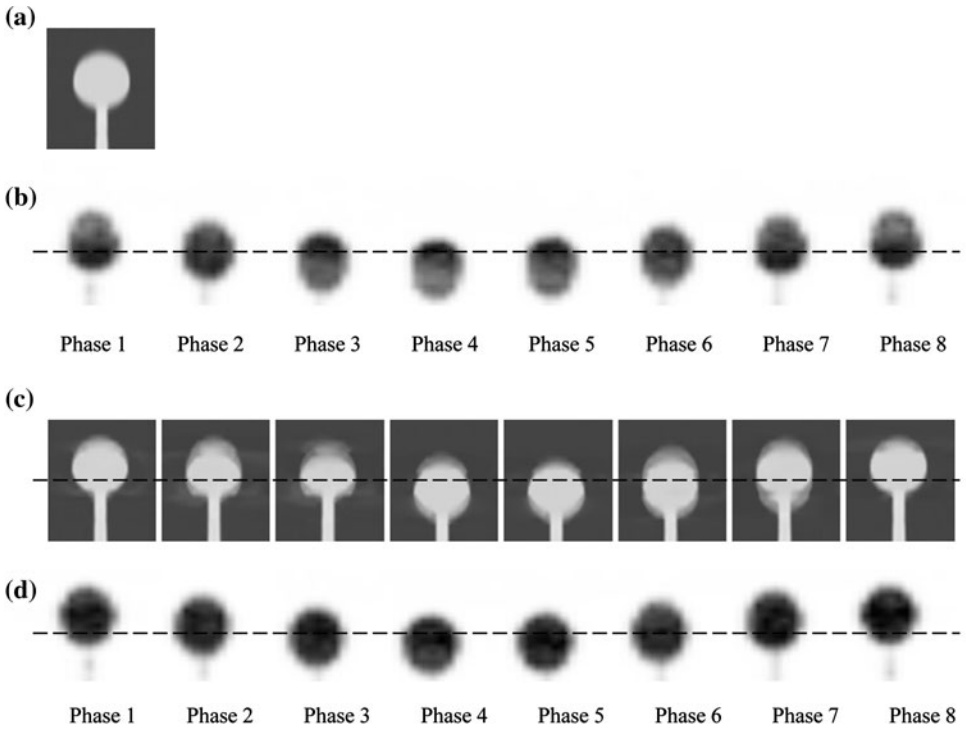

Fig. 3 Gated PET and CT images in respiratory motion. Coronal images of the 37 mm sphere in each respiratory phase are shown; **a** HCT, **b** gPET–HCT, **c** 4DCT and **d** gPET–4DCT. *Broken lines* indicate the center position of the displacement. The radioactivity distribution in the sphere of the gPET–HCT was not homogeneous. The hot area in the sphere differs among phases. That of gPET–4DCT was homogeneous

Table 2 Comparison of sphere dimensions on PET and CT images

	Sphere diameters (mm)						Mean
	10	13	17	22	28	37	
PET							
Nonmotion							
sPET–HCT	11.2	16.5	14.7	4.8	2.4	0.6	8.4
Motion							
sPET–HCT	–	173	151	109	50.2	54.5	89.7*
sPET–SCT	–	172	125	90	49.1	57.8	82.4**
sPET–ACT	–	173	130	97	51.2	55.6	84.5***
gPET–HCT	17.1	44.3	48.2	27.3	19.7	11.7	28.1
gPET–4DCT	8.2	46	38.5	22.2	23.4	11.1	24.9
CT							
Nonmotion							
HCT	14.6	11.4	13.7	11.5	5.8	0.2	9.5
Motion							
SCT	208.1	174.5	149	117.4	80.6	63.1	132.1****
4DCT	62.4	61.5	58.2	44.3	30.5	28.9	30.1

The numbers are the %dimensions in comparison to the actual dimensions

* The mean %dimensions of the sPET–HCT were significantly higher than those of nonmotion sPET–HCT ($p < 0.01$), gPET–HCT ($p < 0.05$), and gPET–4DCT ($p < 0.01$)

** The mean %dimensions of the sPET–SCT were significantly higher than those of nonmotion sPET–HCT ($p < 0.01$), gPET–HCT ($p < 0.05$), and gPET–4DCT ($p < 0.05$)

*** The mean %dimensions of the sPET–ACT were significantly higher than those of nonmotion sPET–HCT ($p < 0.01$), gPET–HCT ($p < 0.05$), and gPET–4DCT ($p < 0.05$)

**** The mean %dimensions of the SCT were significantly higher than those of nonmotion HCT ($p < 0.01$) and 4DCT ($p < 0.01$)

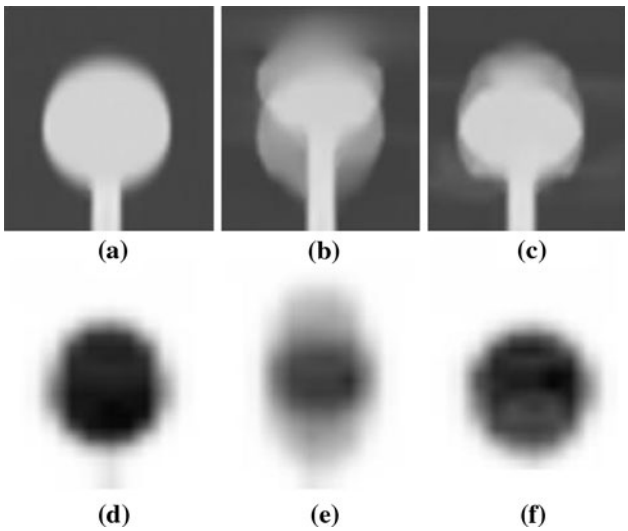

Fig. 4 CT and PET images. In comparison with the nonmotion HCT image (**a**), the SCT image blurs due to motion (**b**). The 4DCT image shows only a little blurring (**c**). In comparison with the PET image of sPET–HCT in nonmotion (**d**), that of the sPET–SCT appears to be blurred (**e**). The gPET–4DCT appears to be less blurred (**f**)

Discussion

This study examined the usefulness of gated CT acquisition for the quantification of gated PET/CT by comparing a different acquisition protocol using a moving hot sphere phantom.

In nonmotion, the RCs of the sPET–HCT were more than 90% in the spheres with diameters of at least 17 mm.

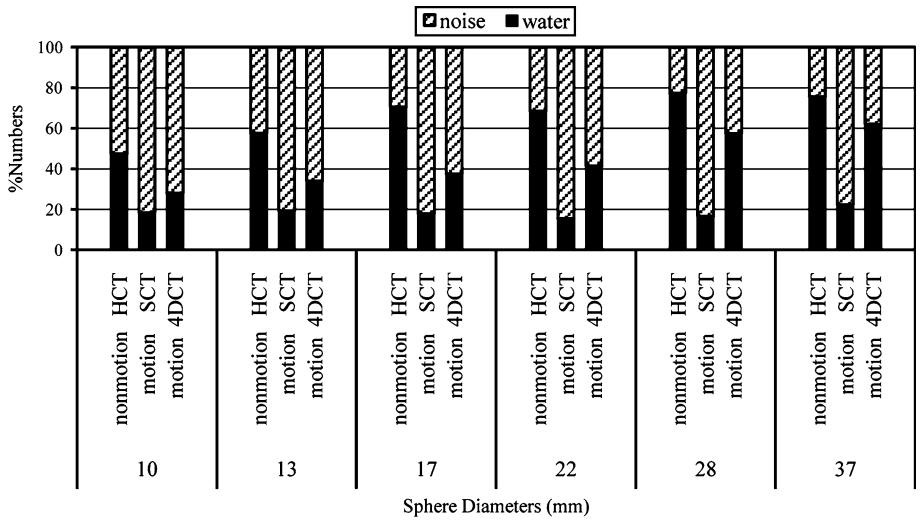

Fig. 5 The %numbers of pixels with CT numbers for water density and noise density in different CT scan modes

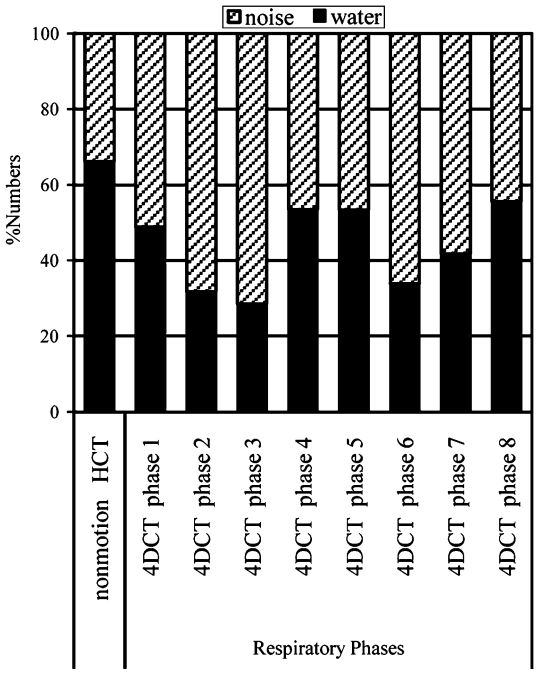

Fig. 6 The %numbers of pixels with CT numbers for water density and noise density in each respiratory phase of 4DCT. The %numbers shows the mean of all spheres

In motion, the PET counts decreased with motion. Furthermore, the smaller the sphere size, the more the PET counts decreased. Pevsner et al. [11] also compared the maximum radioactivity of spheres in motion with a displacement of 2 cm with those in nonmotion. They reported that the RCs of 13 and 22 mm spheres in motion were underestimated by as much as 75 and 40%, respectively. Okubo et al. [12] examined the quantification of PET/CT using a moving phantom oscillating with a displacement of 10, 20, and 30 mm. They reported that the SUV_{max} of 22 and 28 mm spheres also decreased when the displacement was 30 mm. The PET counts in motion decreased because the PET counts of the sphere were distributed into the widely smeared area determined by both the sphere diameter and displacement distance. This phenomenon was caused by the overlap in PET emission data interacting between the sphere diameter and the displacement distance.

The %counts of the sPET–HCT, sPET–SCT, and sPET–ACT markedly decreased in motion, while those of the gPET–HCT and gPET–4DCT mildly decreased. The gated PET acquisition is thus considered to improve the dispersion of radioactivity in comparison with the static PET acquisition. Nehmeh et al. [8] evaluated the effect of gated acquisition on motion-induced underestimation using an oscillating point source. They reported that the gated acquisition improved the distribution of radioactivity. Vines et al. [13] compared the static PET acquisition in motion to the gated PET acquisition in motion. They reported that the PET counts of gated PET in motion, compared with those of static PET in motion, were closer to those of static PET in nonmotion. These results suggest that the gated acquisition of PET is necessary to obtain an accurate PET count in motion. Although the gPET–4DCT improved quantitative accuracy, it could not obtain complete recovery in comparison to the sPET–HCT in nonmotion in this study. The difference may be due to the residual movement of the spheres during respiratory phases in spite of the gated acquisition. Another possibility is the short acquisition time of gPET (1 min/phase × 8 phases = 8 min), resulting in an increase of statistical variance.

CTAC is also important for the quantification of PET. Some clinical studies have reported that the misregistration

between PET emission data and CTAC caused the underestimation of PET counts. Erdi et al. [4] reported that misregistration between PET emission data and CTAC resulted in SUV variability of up to 30%. Some studies have reported that the application of both SCT and ACT for CTAC was useful for improving quantification [6, 7]. However, the present results showed that the underestimation of PET counts could not be improved even when SCT or ACT was used for CTAC. Both SCT and ACT include the motion of several respiratory cycles and provide density-averaged CT images because they were performed with a long rotation time and fixed cine duration images, respectively. Because SCT decreased the %numbers for water density, while conversely increasing that for noise density, the CTAC of SCT might therefore not reflect the actual attenuation map of the sphere. Chi et al. [7] proposed an ACT using 4DCT for attenuation correction with static PET data. They reported that it reduced PET/CT misregistration by matching the temporal resolution between PET and CT data. Although the misregistration between PET emission data and CTAC of SCT and ACT was minimized, the PET counts did not improve when either SCT or ACT was used for CTAC. In addition, neither sPET–SCT nor sPET–ACT improved the underestimation of radioactivity or the overestimation of tumor volume in the static PET in motion. As a result, both SCT and ACT were considered inadequate for CTAC.

The gated PET with 4DCT improved the quantification of PET images in respiratory motion. Although the 4DCT images showed slightly lower water density than HCT, the %counts for gPET–4DCT were better than those for gPET–HCT. This is thought to result from the better image registration of 4DCT to gated PET images at each respiratory phase. In a recent study with gated PET acquisition, Nagel et al. [14] evaluated the potential of 4DCT to improve PET counts in comparison with HCT. They found that 4DCT resulted in improved PET counts of up to 28%. In the present study, the radioactivity distribution of the gPET–HCT images was not homogeneous. The highest radioactive area in the sphere was observed in a limited part of the sphere where the PET images and the CTAC were spatially matched. The highest radioactive area in the sphere was located in a different part from phase to phase. The %counts of the central phases were superior to those of the edge phases. On the other hand, the %counts of the central phases were inferior to those of the edge phase in the gPET–4DCT. Although the PET images and CTAC showed good registration at each phase in gPET–4DCT, the displacement of the edge phases was smaller than that of the central phases. The differences in the degree of blurring are considered to cause the different %counts among phases. However, the distribution of radioactivity in gPET–4DCT was relatively homogeneous, and the difference in the %counts among phases was minimal. Therefore, the gated acquisition of both PET and CT is considered the best acquisition protocol in motion in this study.

The phantom background in this study was filled with air because we were simulating human lung tumor. In the case of abdominal tumors with respiratory motion, we must consider the result when the phantom background is filled with water. The density inside the phantom must be homogeneous and around water density because the phantom consists of only water and the phantom wall. We can ignore the partial volume effect on the CT images of the sphere. Thus, the %numbers should be 100% water density regardless of the different CT protocol. Furthermore, misregistration between PET images and CT images can also be ignored. These factors are thought to increase the PET counts of spheres due to the improved accuracy of attenuation correction. The differences in %counts between the different CT protocols are thought to disappear too. Vines et al. [13] estimated the difference in PET counts among static and gated acquisition in motion and static acquisition in nonmotion with corrected helical CT attenuation. The difference in PET counts between sPET–HCT in nonmotion and gPET–HCT in motion was equal to or less than 10% for spheres more than 17 mm in diameter. This is in agreement with the result for gPET–4DCT in the present study (Table 1).

The gated PET data in this study were divided into eight phases, and the acquisition time of each phase was thus 1 min. The acquisition time of each phase determined by the number of phases and the total acquisition time would have an effect on the quantification of PET data. Motion-induced underestimation would also be different for each tumor size at different displacement distances and sphere background ratios of radioactivity. The respiratory motions of patients are not usually regular, though those in the current phantom study were regular. Further examinations under several different conditions and with clinical trials are required to confirm the general usefulness of gPET–4DCT for quantification.

Conclusions

In respiratory motion, PET acquisition in the static mode underestimated the radioactivity and overestimated the dimensions. Neither SCT nor ACT improved these errors. PET acquisition in the gated mode improved the quantification of PET/CT images, though gated PET acquisition using 4DCT is necessary for further improvement.

Acknowledgments The authors thank Mr. Hirofumi Kawakami (GE Healthcare Japan) and Mr. Naoyuki Tamamura (Nihon Medi-Physics) for their technological assistance.

References

1. Weber WA, Figlin R. Monitoring cancer treatment with PET/CT: does it make a difference? J Nucl Med. 2007;48:36–44.
2. Goerres GW, Kamel E, Heidelberg TN, Schwitter MR, Burger C, von Schulthess GK. PET–CT image co-registration in the thorax: influence of respiration. Eur J Nucl Med. 2002;29:351–60.
3. Cohade C, Osman M, Marshall LT, Wahl RN. PET–CT: accuracy of PET and CT spatial registration of lung lesions. Eur J Nucl Med Mol Imaging. 2003;30:721–6.
4. Erdi YE, Nehmeh SA, Pan T, Pevsner A, Rosenzweig KE, Mageras G, et al. The CT motion quantitation of lung lesions and its impact on PET-measured SUVs. J Nucl Med. 2004;45:1287–92.
5. Lagerwaard FJ, Van Sornsen de Koste JR, Nijssen-Visser MR, Schuchhard-Schipper RH, Oei SS, Munne A, et al. Multiple "slow" CT scans for incorporating lung tumor mobility in radiotherapy planning. Int J Radiat Oncol Biol Phys. 2001;51:932–7.
6. Nye JA, Esteves F, Votaw JR. Minimizing artifacts resulting from respiratory and cardiac motion by optimization of the transmission scan in cardiac PET/CT. Med Phys. 2007;34:1901–6.
7. Chi PC, Mawlawi O, Nehmeh SA, Erdi YE, Balter PA, Luo D, et al. Design of respiratory averaged CT for attenuation correction if the PET data from PET/CT. Med Phys. 2007;34:2039–47.
8. Nehmeh SA, Erdi YE, Ling CC, Rosenzweig KE, Squire OD, Braban LE, et al. Effect of respiratory gating on reducing lung motion artifacts in PET imaging of lung cancer. Med Phys. 2002;29:366–71.
9. Nehmeh SA, Erdi YE, Pan T, Yorke E, Mageras GS, Rosenzweig KE, et al. Quantitation of respiratory motion during 4D-PET/CT acquisition. Med Phys. 2004;31:1333–8.
10. Pan T, Lee TY, Rietzel E, Chen GT. 4D-CT imaging of a volume influenced by respiratory motion on multi-slice CT. Med Phys. 2004;31:333–40.
11. Pevsner A, Nehmeh SA, Humm JL, Mageras GS, Erdi YE. Effect of motion on tracer activity determination in CT attenuation corrected PET images: a lung phantom study. Med Phys. 2005;32:2358–62.
12. Okubo M, Nishimura Y, Nakamatsu K, Okumura M, Shibata T, Kanamori S, et al. Static and moving phantom studies for radiation treatment planning in a positron emission tomography and computed tomography (PET/CT) system. Ann Nucl Med. 2008;22:579–86.
13. Vines DC, Keller H, Hoisak JDP, Breen SL. Quantitative PET comparing gated with nongated acquisitions using a NEMA phantom with respiratory-simulated motion. J Nucl Med Technol. 2007;35:246–51.
14. Nagel CC, Bosmans G, Dekker AL, Ollers MC, Ruysscher DK, Lambin P, et al. Phased attenuation correction in respiratory correlated computed tomography/positron emitted tomography. Med Phys. 2006;33:1840–7.